Geomechanics and Engineering, *Vol. 32, No. 2 (2023) 209-232*
https://doi.org/10.12989/gae.2023.32.2.209

Investigation on economical method of foundation construction on soft soils in seismic zones: A case study in southern Iran

Javad Jalili*, Farajdollah Askari[a], Ebrahim Haghshenas[b] and Azadeh Marghaiezadeh[c]

International Institute of Earthquake Engineering and Seismology, No.21, Arghavan St., Northern Dibaji St., Lavasani Ave., Tehran 19395/3913, Iran

(*Received August 24, 2022, Revised December 31, 2022, Accepted January 9, 2023*)

Abstract. A comprehensive study was conducted to design economical foundations for a number of buildings on soft cohesive soil in the southern coastal regions of Iran. Both static and seismic loads were considered in the design process. Cyclic experiments indicated that the cohesive soil of the area has potential for softening. Consequently, the major challenge in the design stages was relatively high dimensions of settlement, under both static and seismic loadings. Routine soil-improvement methods were too costly for the vast area of the project. After detailed numerical modeling of different scenarios, we concluded that, in following a performance-based design approach and applying a special time schedule of construction, most of the settlement would dissipate during the construction of the buildings. Making the foundation as rigid as possible was another way to prevent any probable differential settlement. Stiff subgrade of stone and lime mortar under the grid foundation and a reinforced concrete slab on the foundation were considered as appropriate to this effect. In favor of an economical design, in case the design earthquake strikes the site, the estimations indicate no collapse of the buildings even if considerable uniform settlements may occur. This is a considerable alternative design to costly soil-improvement methods.

Keywords: compressible soil; cyclic softening; dynamic numerical analysis; grid foundation; performance-based design; rigid foundation; soil improvement

1. Introduction

Iran is located on the seismic belt running around the earth. There is a variety of geological settings in this country, including soft saturated soils in coastal regions of the country. Construction of building foundations which are safely designed for such adverse conditions is usually costly. This paper reports on a recent study in the coastal lands of Khuzestan province in the south of Iran. The project area is located within the southern margin of Khuzestan alluvial plain along the northern parts of the Persian Gulf seashore (Khour-e-Mosa). The delta land consists of hundreds of meters of young and quaternary deposits built mainly of alternate layers of low-plastic clay, silt and sand (Zamiran 2002). Fig. 1 shows the location of the project. High level of ground water along with the soft nature of the superficial soil deposits have brought about a soft saturated base for foundation design and construction.

According to Iranian Code of Practice for Seismic Resistant Design of Buildings (2014), the project area is characterized by relatively low seismicity with base acceleration of 0.2g. However, the highly compressible subsoils with low bearing capacity led to the excessive structure settlement even under static construction surcharge. The laboratory experiments also indicated the potential of cyclic softening of the soil.

There is detailed literature on construction on soft soils. We considered the most practical improvement methods for the soil in the project area to pick a useful alternative to the design method, which is proposed in this study. A detailed review of the ground improvement methods was performed by the authors, which is out of the scope of the manuscript to be reported herein. Thus, we arrived at the method intended to be used from among several alternatives including: combined surcharge and vacuum preloading, deep mixing, grouting by injection, vibrating stone columns, geogrid-encased sand columns, pre-cast concrete piling and prefabricated vertical drains (Schaefer 2016, Karstunen and Leoni 2008). Eventually, several attempts were made to countermeasure the excessive settlement by treating the soil beneath each foundation individually, as will be described in Section 4, with the aim of avoiding considerable extra costs. However, none of the soil-improvement methods that are practically applied to the whole project area could be performed due to the high cost of such treatments for the vast area of this study. Most of other treatments that could be individually applied under each building foundation, as will be pointed out in Section 4, also turned out unsuccessful. Finally, based on a performance-based design approach, a construction schedule along with some foundation-stiffening methods were recommended, as will be described in the paper.

While examining different alternatives to have a safe design of foundations, both mat and grid foundations were

*Corresponding author, Assistant Professor
E-mail: jalili@iiees.ac.ir
[a]Associate Professor
[b]Associate Professor
[c]Research Expert

ISSN: 2005-307X (Print), 2092-6219 (Online)

Fig. 1 Location of the project area

considered in this study. Mat foundations are used when more than half of the ground surface is covered by conventional spread footings (Bowles 1996). Heavy column loads along with weak subsoil condition usually prefer mat foundations. Day (2010) considers mat foundation as an alternative to shallow foundations on improved soil, to mitigate earthquake effects. Coduto *et al*. (2014) state that a three-dimensional finite element analysis including the mat, the underlying soil and the superstructure is an accurate representation of the mat, facilitating a precise and economical design of the foundation. We applied this form of modeling in this study, benefiting also from grid foundation.

Grid foundations are known to be alternatives to mat foundations when it is not necessary to cover the whole area to provide bearing capacity. Even though grid foundations are similar in plan to the tied strip footings, care must be taken that grids have flexural rigidity at both longitudinal and lateral dimensions, in contrast to tied strip foundations that do not have considerable flexural rigidity along the ties. The settlement of grid foundations is calculated in the same manner as that of a mat and their bearing capacity is figured out as strip footings (Fakher 2011).

Hodgkinson (2013) also describes many kinds of mat foundations as a series of strip foundations that are tied together by means of a ground slab. He recommends such tied strip foundations to be used only under light loads, such as two-story residential structures, employing simple strip foundation calculations. He also points out that stress concentration occurs at the edges of the mat foundation, increasing the potential of shear failure there, which should necessarily be inspected while designing the mats.

When perusing the literature on grid foundations, multi-edge shallow foundations (i.e., T-shaped, H-shaped or cross-shaped) also appear as important. Ghazavi et al. have conducted several experiments and numerical analyses of multi-edge shallow foundations, obtaining the main finding that interference of shear zones in the voids of multi-edge foundations (as, for instance, around the adjacent parts of a cross-shaped foundation) leads to higher bearing capacity. Importantly, there is an optimal distance between two adjacent strip foundations that leads to capacity-increasing interferences. (Ghazavi and Hadiani, 2005, Ghazavi and Mokhtari, 2008).

Based on the literature, as grid foundations may also benefit from shear-zone interference, they can have better performance compared with mat foundations, if the proper geometry is provided (Jalili *et al.* 2022). Consequently, the usefulness of grid foundation in the adverse conditions of the project site was subjected to investigation in this study.

The structure of the paper coincides the steps of the study:

- *Subsurface investigations (Section 2):* detailed soil investigation was required to precisely define the bearing capacity and settlement of the building foundations.
- *Analytical design of foundations (Section 3):* bearing capacity and allowable settlement were evaluated by classical hand calculations, leading to limited allowable loading on foundations. Some treatment was needed to increase the allowable capacity of foundations to meet the project requirements.
- *Numerical analyses to design foundations (Section 4):* different treatments were simulated numerically. Both static and seismic loadings were considered. It was observed that some known treatments (such as short stone-columns) may not reduce the seismic settlement when they are floating in soft soils. There was not an economical way to reduce the settlements!
- *Factor of safety against cyclic softening (Section 5):* excessive static and seismic settlements were calculated in numerical analyses. The static portion was in line with hand calculations in Section 3. The seismic settlements were hand calculated in this section and the results confirmed numerical results.
- *Field evidence of the behavior of different types of foundations (Section 6):* observations from a neighboring site that experienced earthquakes showed that the main conclusion of the study is practical: Stiff structures tolerated excessive settlements and did not collapse, despite damaged buildings that were not constructed stiff enough to tolerate seismic settlements.
- *Concluding remarks (Section 7):* Results of Section 4, that was confirmed by Sections 3 and 5, showed that the only economical and practical solution was to make the structure (especially the foundation) as rigid as possible with scheduled construction stages to dissipate the extra settlement during construction. Experiences reported in Section 6 confirmed this conclusion.

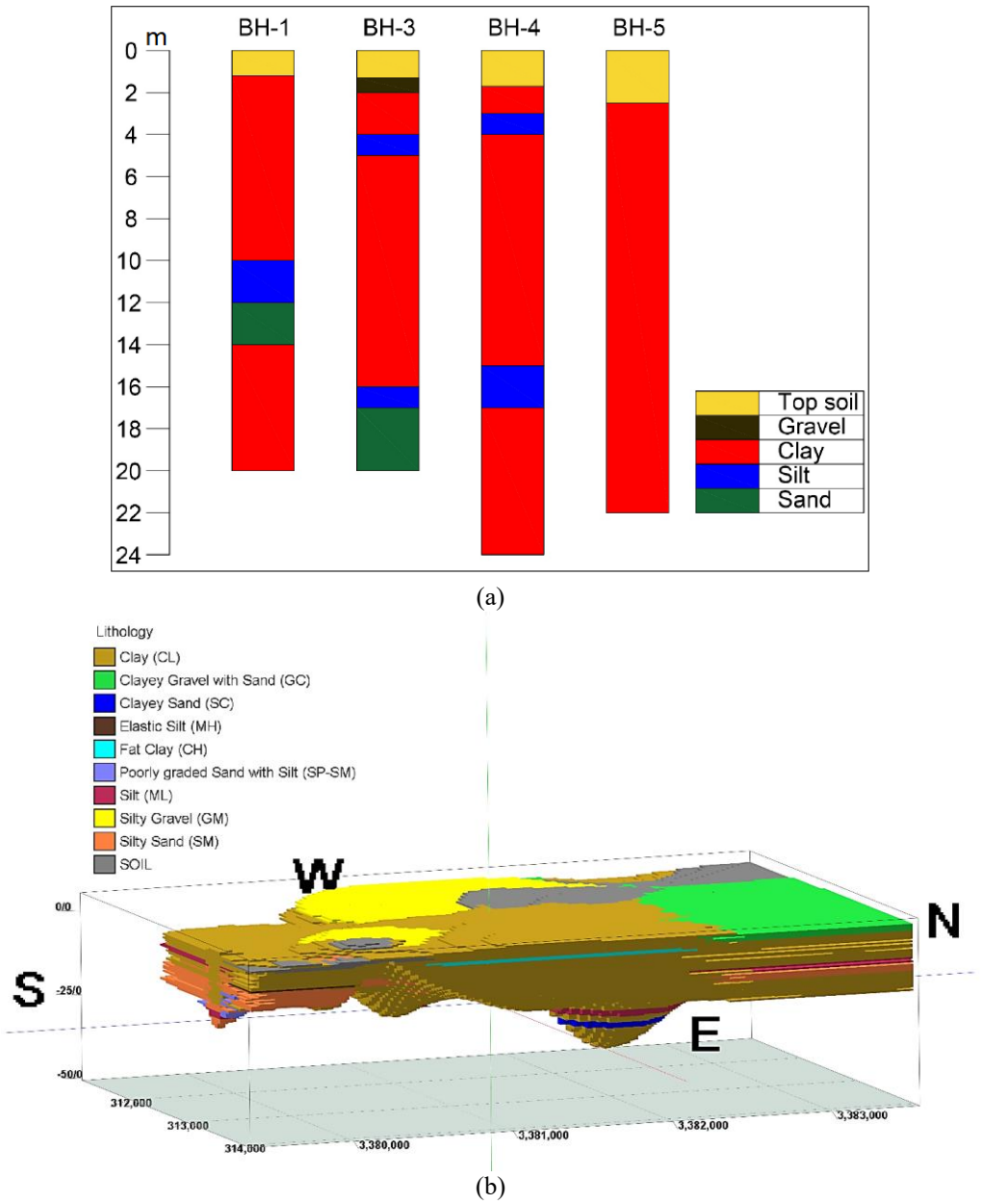

Fig. 2 Site investigation results: (a) Typical borehole diagrams (SakhtAzma 2021); (b) Soil layering of the project area from the surface down to the depth of drilling, 15 to 50 meters - View from the east

2. Subsurface investigations

A detailed site characterization was performed as part of the comprehensive studies on the site of the region to design safe structures (Jalili *et al.* 2021). The investigation included laboratory experiments on undisturbed samples taken from the field. Consolidation and static shear strength experiments revealed the high compressibility of the subsoil (Sakhtazma 2021). Dynamic triaxial tests on the samples showed the tendency of the saturated samples to softening (Jalili *et al.* 2021).

Five typical borehole diagrams among eighteen drilled boreholes in the area, and the layering of the site are shown in Fig. 2. The layering in Fig. 2(b) was generated by Rockworks software, after defining the boreholes' data in the code. The depth of the layers in this Figure is equal to the related borehole depth on the site. It is shown in this Figure that the majority of the site is covered with low-plastic clays. Water table nearly coincided 2 meters below the ground surface along the area. Defining the deformation and strength parameters of the site-soil was next needed for the purposes of the design.

2.1 Deformation and shear strength parameters

To design foundations, both deformation and strength parameters are required. Plenty of in situ and laboratory tests were conducted by SakhtAzma consulting corporation (2021) including standard penetration test (SPT), Vane shear test on the site as well as consolidation and triaxial

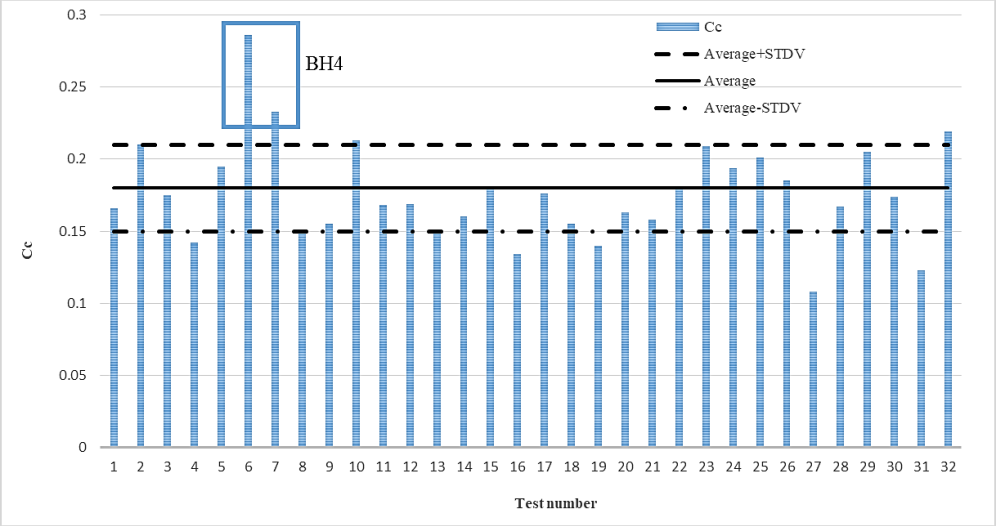

Fig. 3 C_c parameters resulted from 32 consolidation tests on samples taken from 18 drilled boreholes (BH1 to BH18) across the project area (Cc average=0.18; see the solid line)

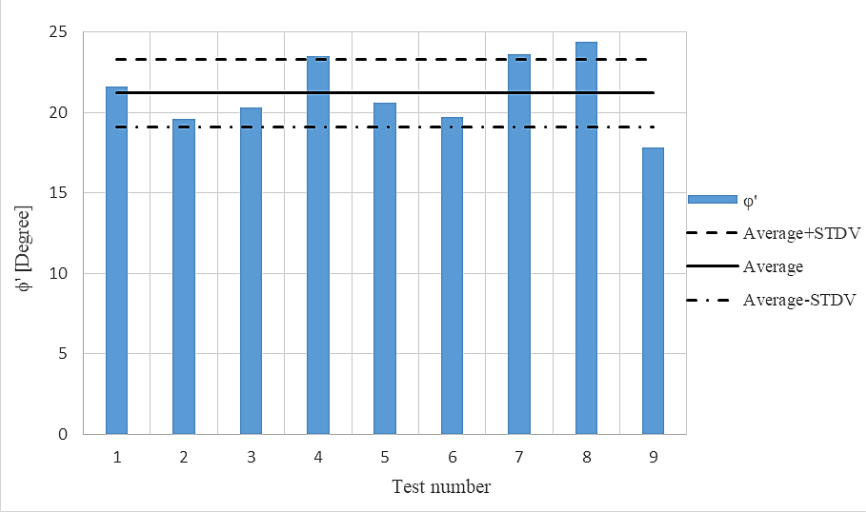

Fig. 4 Mohr-Coulomb strength parameters resulted from 9 CU triaxial tests on samples taken across the project area (effective friction angle: $\varphi'_{average}$=21.2°; see the solid line)

tests on undisturbed samples at laboratory.

Fig. 3 shows the variation of compression index (C_c[1]) from 32 consolidation tests on the samples taken from 18 drilled boreholes (BH1 to BH18) across the entire site (SakhtAzma 2021). As shown in this figure, the maximum values of Cc are found to be in borehole BH4, i.e., one among eighteen drilled boreholes. Given the parameter variation shown in Fig. 3, C_c=0.17 was selected for foundation design on the project site.

Figs. 4 and 5 also show variation of Mohr-Coulomb strength parameters, i.e., effective friction angle and effective cohesion (Eq. (1) to Eq. (5)) from the consolidated-undrained triaxial tests, respectively.

$$\tau=\sigma'*\tan(\varphi') +C' \quad \text{Mohr-Coulomb failure line} \quad (1)$$

$$\sigma'= \sigma-u \quad \text{effective normal stress} \quad (2)$$

$$\varphi' \quad \text{effective angle of friction} \quad (3)$$

$$C'= C-u \quad \text{effective cohesion} \quad (4)$$

$$u \quad \text{excess pore water pressure} \quad (5)$$

The undrained strength measured from total stress results of the CU tests was in the range of 5 to 35 kPa, being coincident with the average of the Vane shear-test results, i.e., 25 kPa (SakhtAzma 2021). For the effective strength parameters, C'=21 kPa and ϕ'=20° were selected based on the threshold, i.e., the area between the dashed and dash-dotted lines shown in Figs. 4 and 5.

[1] Cc is the tangent of the straight-line part of the semi log plot of void ratio versus log pressure

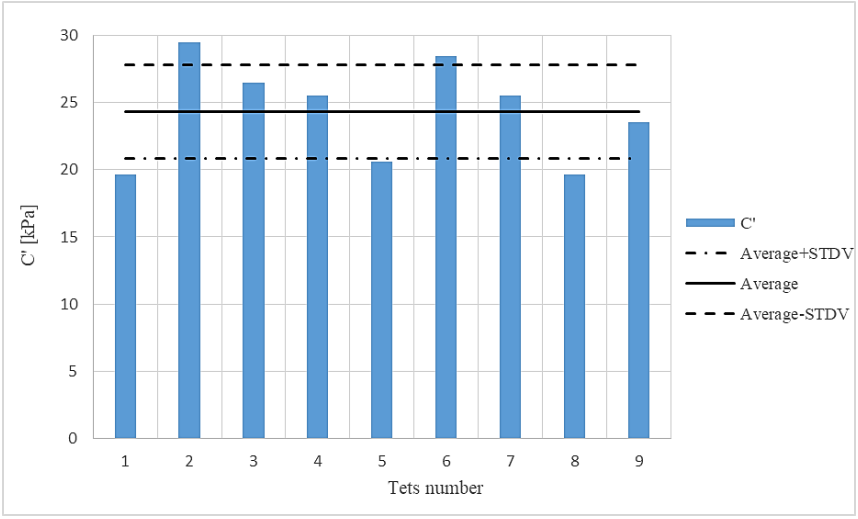

Fig. 5 Mohr-Coulomb strength parameters resulted from 9 CU triaxial tests on samples taken across the project area (effective cohesion: $C'_{average}$=24.3 kPa; see the solid line)

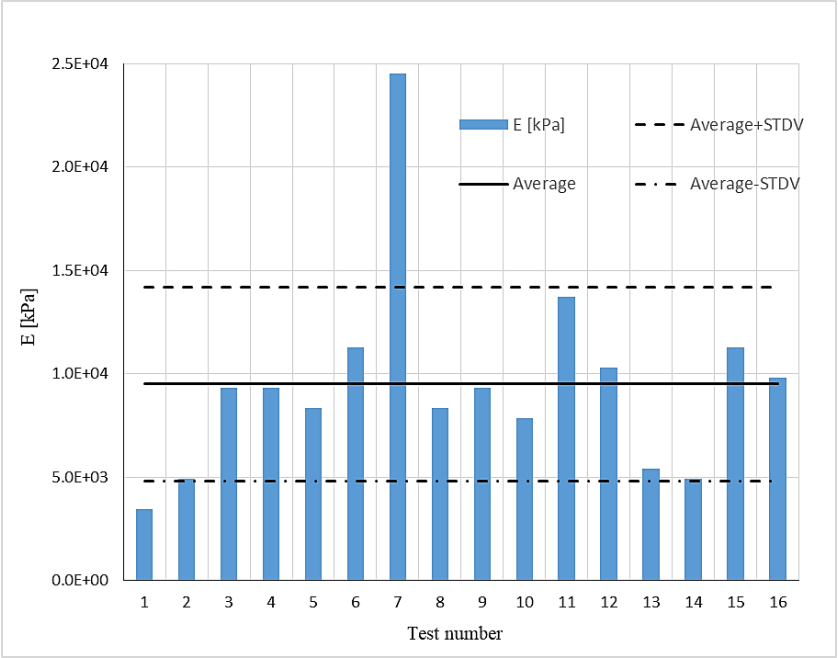

Fig. 6 Modulus of deformation estimated from correlations related to the tests on samples taken across the project area and also plate-load test on the site ($E_{average}$=9500 kPa)

For modulus of deformation evaluation, the correlations with the SPT values obtained on the site were used. Fig. 6 shows the magnitudes calculated for selective boreholes across the site. Since the deformability of the soil was a matter of concern in the site area, preference of the modulus deformation was selected by the aid of complementary static consolidated undrained triaxial tests conducted on the undisturbed samples from the site by the authors.

Fig. 7 shows the results of one of the complementary static triaxial tests conducted by the authors. Given these results and their consistency with the threshold values in Fig. 6, E=5000 kPa was preferred for the calculations of the foundation settlement. In this figure, deviator stress is defined by Eq. (6).

$$q: \text{deviator stress in triaxial test} = \sigma_1 - \sigma_3 \quad (6)$$

$$r_u : \text{excess pore water pressure ratio} = u/\sigma'_{3c} \quad (7)$$

σ'_{3c}: consolidation pressure

It should be noted that attempts were made to suggest parameter-zonation across the project area by geographic information system mapping. However, this was not successful due to the random distribution of the parameter magnitudes across the site. The random distribution is a characterization of alluvial deposits in the delta lands (Khour-e-Mosa in Fig. 1).

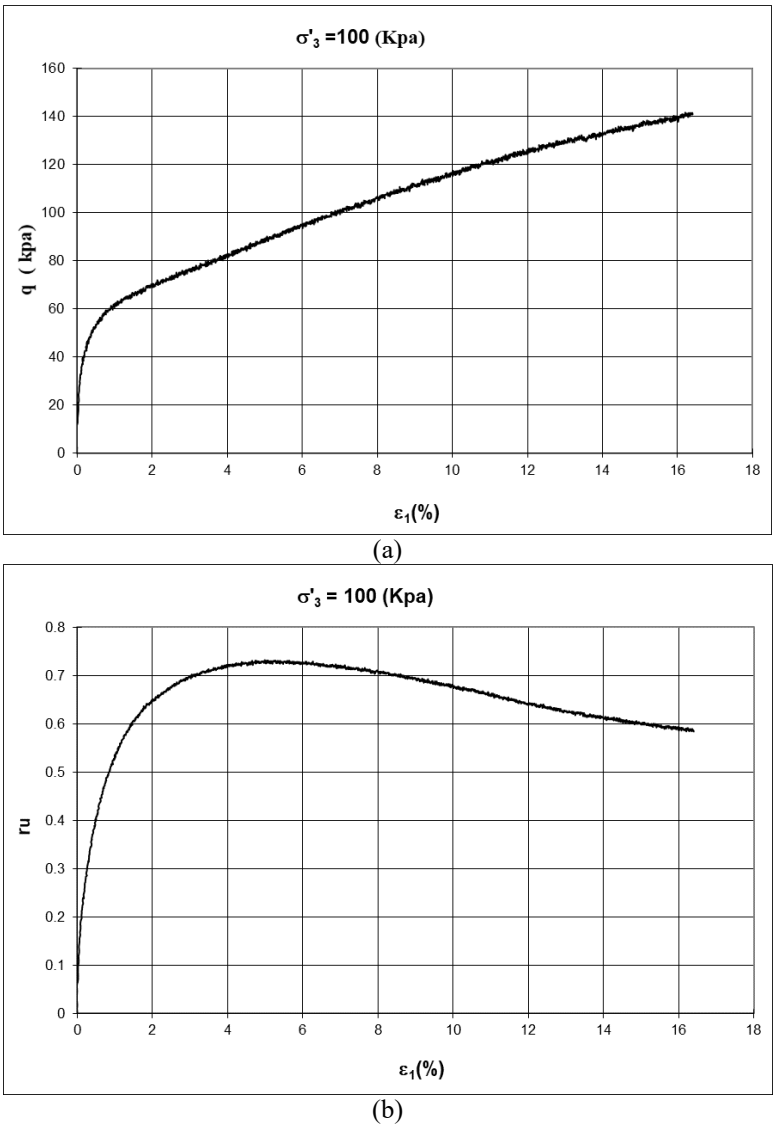

Fig. 7 Sample of a complementary static consolidated undrained triaxial test result: (a) deviator stress versus axial strain and (b) excess pore water pressure ratio versus axial strain

2.2 Cyclic softening susceptibility

According to the most of the criteria for liquefaction susceptibility, the soil of the project area was not liquefiable due to the massive clayey consistency. However, in line with the recommendations by Seed *et al*. (2003), we performed cyclic triaxial tests on the undisturbed soil samples to verify softening susceptibility (Boulanger and Idriss 2007). To examine the necessity of performing cyclic tests, the index properties of several samples were plotted, as presented in Figs. 8 and 9.

Fig. 8 shows that nearly all of the samples taken from the site have clay-like behavior. In Fig. 9, it is observed that the soil is susceptible to liquefaction, that is softening, so it requires testing (Boulanger and Idriss 2004).

Fig. 9 shows the results of one of the cyclic tests. Nine dynamic CU triaxial tests were conducted to find the cyclic resistance of the soil, which was finally defined as 0.25 in 15 cycles, as shown in Eq. (8). The specimen was cycled until it experienced 3.5% axial strain (single amplitude), which was defined as the softening criterion.

$$\text{Cyclic Resistance Ratio (CRR)} = \frac{q}{2\sigma'_3} = 0.25 \qquad (8)$$

3. Analytical design of foundation

As the first step, the ultimate bearing capacity of the foundations on the soil defined in Table 1 was computed based on the Hansen's bearing capacity equations for shear failure (Bowles 1996). Then, the bearing capacity that causes 10 cm allowable settlement was calculated. Lastly, these analytical solutions were evaluated by the finite element analyses of one-story to four-story building models.

Fig. 11 shows the ultimate bearing capacity of the mat and grid foundation by Hansen's equations. Fig. 12 shows the allowable bearing capacity leading to 10 cm settlement,

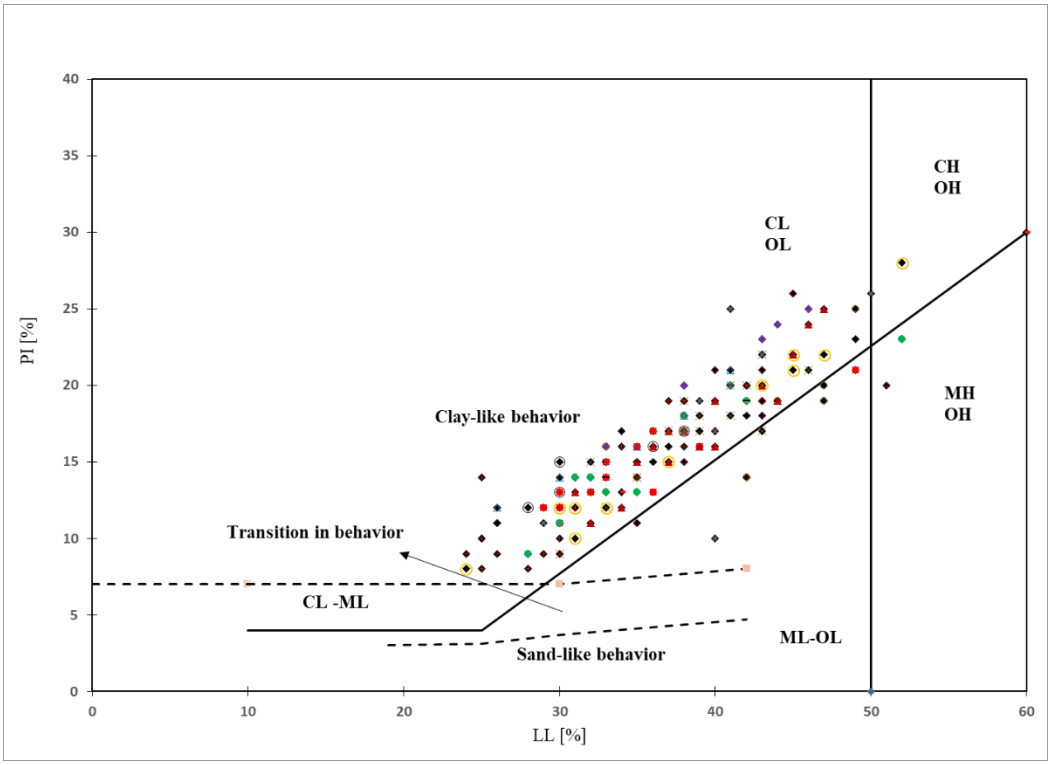

Fig. 8 Plasticity index and liquid limit of the samples taken from the field area of the project to categorize its behavior

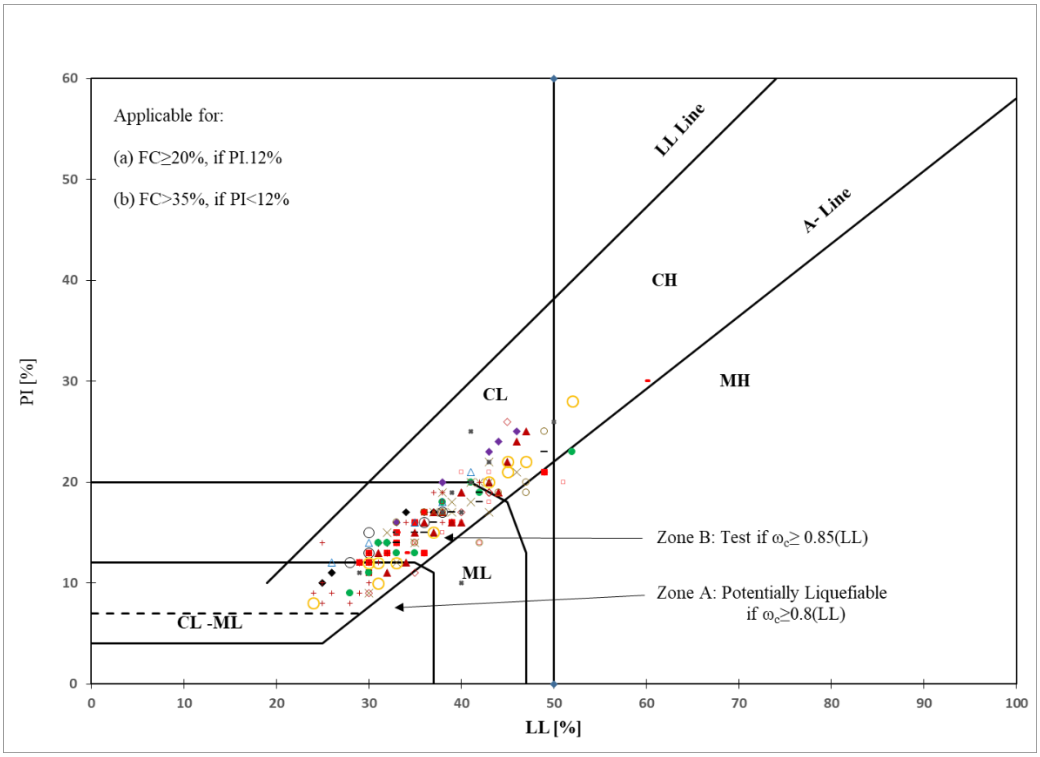

Fig. 9 Plasticity index and liquid limit of the samples taken from the field area of the project to inspect triggering of cyclic failure

taking into account both immediate and consolidation settlements.

The issues of defining a factor of safety equal to 3 and dividing the magnitudes in Fig. 11 to this factor of safety results in the curves of allowable bearing capacity originating from shear failure. Fig. 12 also shows allowable bearing capacity originating from allowable settlement. As can be clearly seen in Figs. 11 and 12, the settlement-based

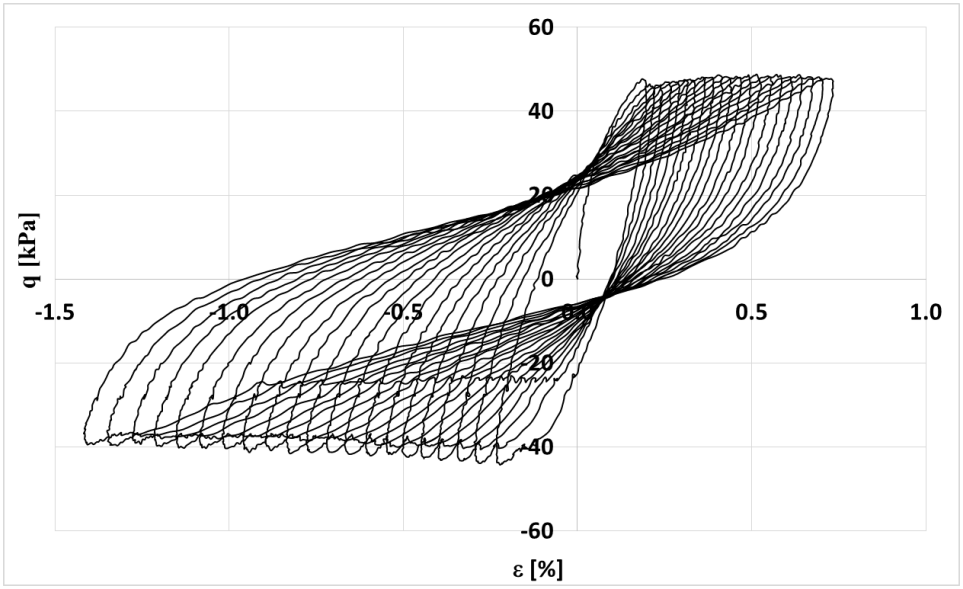

(a)

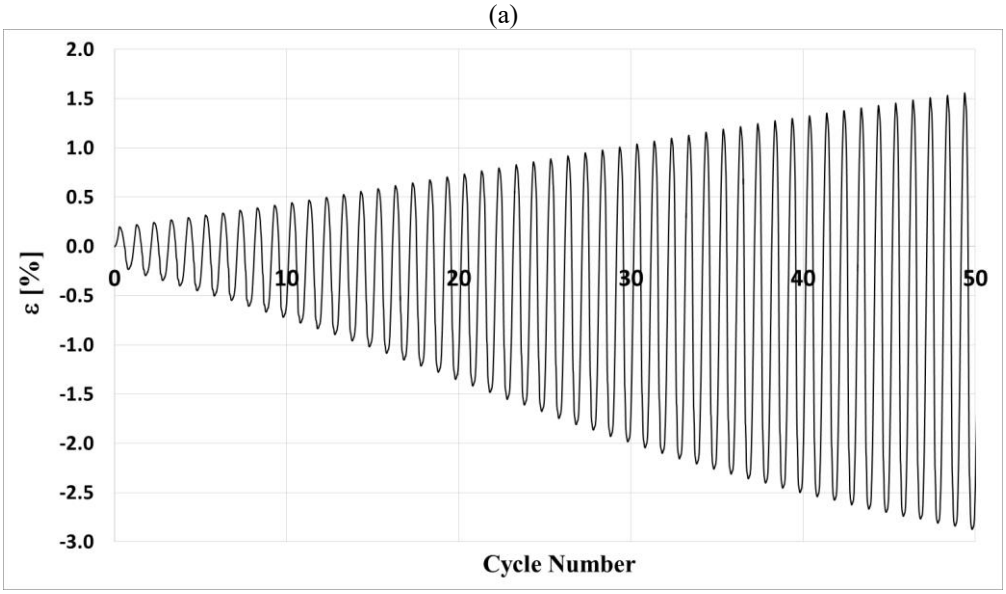

(b)

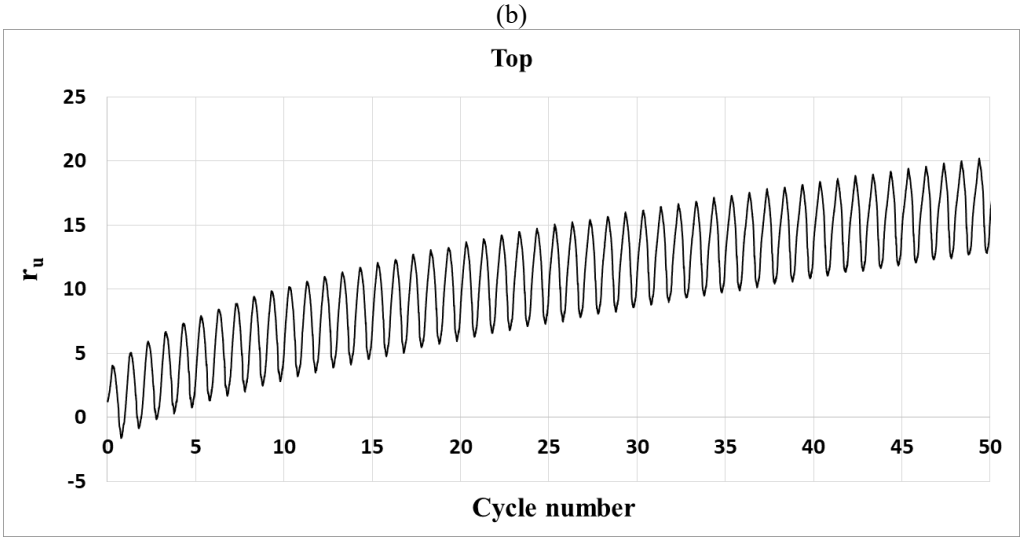

(c)

Fig. 10 Sample of stress-controlled cyclic consolidated undrained triaxial test result: (a) Deviator stress versus axial strain, (b) axial strain versus cycle number, (c) excess pore water pressure at top of the specimen and (d) excess pore water pressure at bottom of the specimen

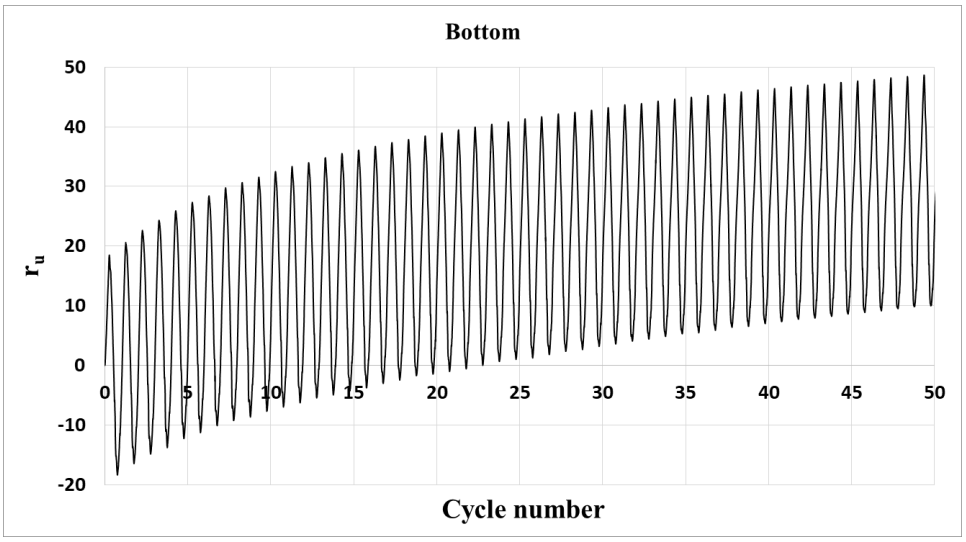

(d)

Fig. 10 Continued

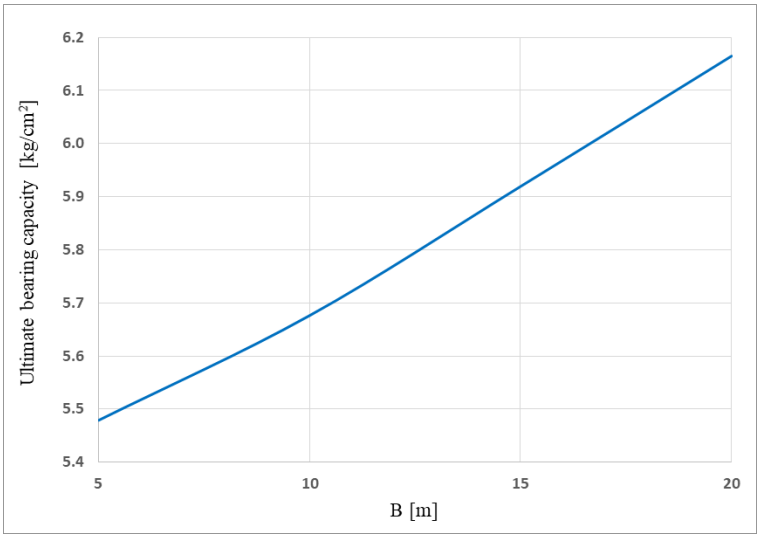

(a)

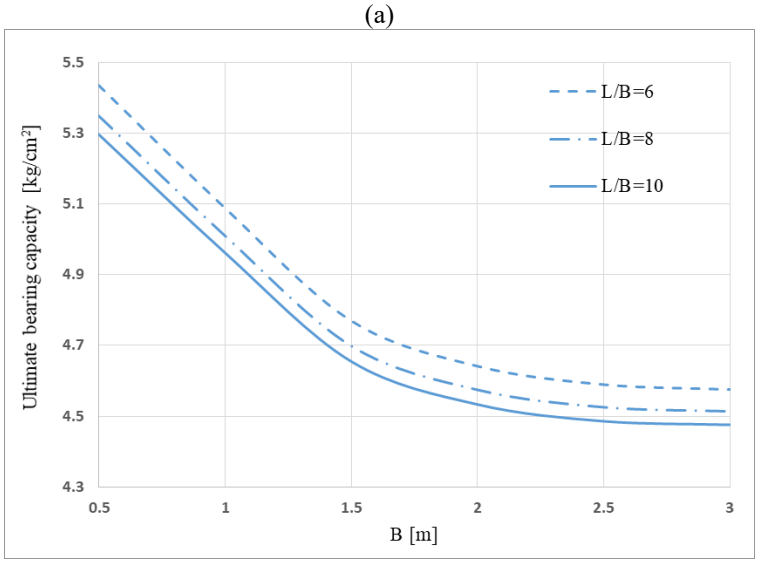

(b)

Fig. 11 Ultimate bearing capacity of: (a) mat foundations and (b) grid foundations (B=foundation width, L=foundation length), based on Hansen's equations

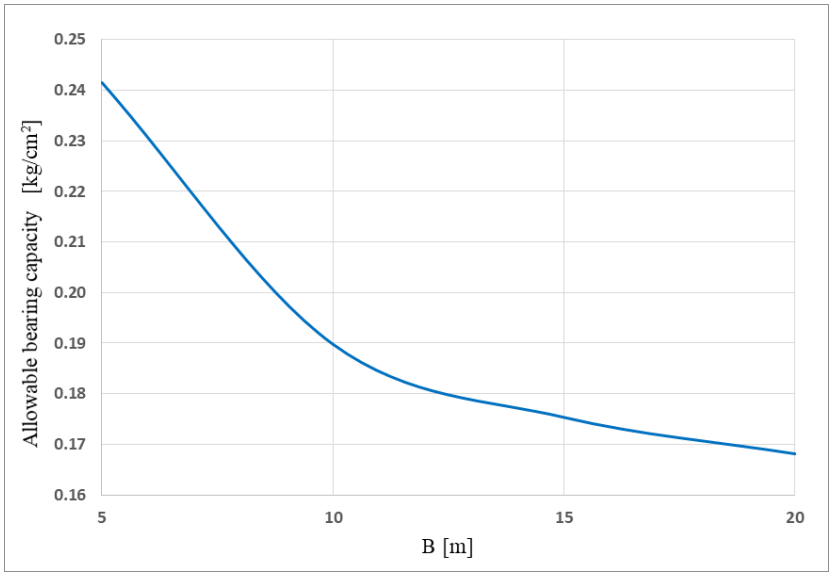

(a)

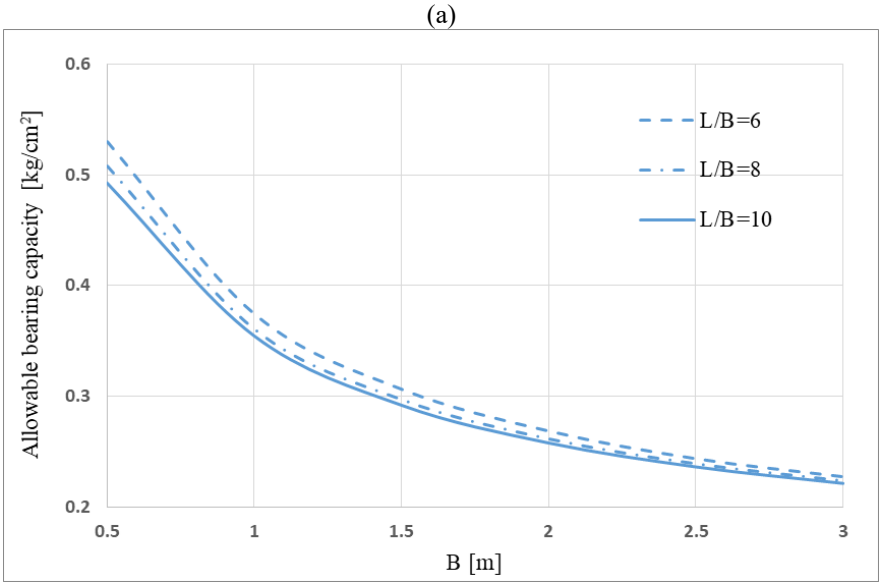

(b)

Fig. 12 Allowable bearing capacity of: (a) mat foundations and (b) grid foundations (B=foundation width, L=foundation length) leading to 10 cm allowable settlement including consolidation

Table 1 Parameters for the design of foundations

Parameter	Definition	Unit	Magnitude
ϕ'	angle of friction	°	20
C'	cohesion	kPa	21
E	deformation modulus	kPa	5000
Cc	compression index	-	0.17
CRR	cyclic resistance ratio	-	0.25

allowable capacity is substantially lower than the allowable capacity obtained from shear strength equations. The reason behind is the considerable amount of consolidation settlement.

Since the result of the analytical design would limit the number of the stories of the buildings, the authors investigated the situation further by means of numerical analyses.

Table. 1 includes the parameters selected for the design of foundations.

Given the analytical designs in Figs. 11 and 12 as well as an estimate of 0.1 kg/cm^2 for each story of the buildings, we can conclude that it is not possible to build higher than two-story buildings on mat foundations and four-story buildings on grid foundations with B=1 m. This is a preliminary conclusion resulting from the static design of the foundation while seismic considerations have not been involved in the design, yet. Importantly, however, the current routine of building construction on the site has been successful over the recent 20 years for numerous one to five-storey buildings, though fortunately without any occurrence of strong earthquakes. Fig. 13 shows a typical subgrade for a grid foundation, designed formerly by local engineers for the area of the project. A layer of stone covered with lime mortar is first built on level ground (or

Fig. 13 Typical subgrade construction on the site consisting of stone mixed with lime mortar

Fig. 14 Five-story buildings constructed across the area of the project with no evidence of excessive settlements during the past 20 years

ground excavated to a depth of 0.5 to 1 m). Then, the reinforced concrete foundation is built on the subgrade. As shown in Fig. 14, several five-story buildings have been constructed over the last 20 years showing no evidence of excessive settlements.

According to the range of values of coefficient of consolidation (c_v[2]) evaluated by SakhtAzma corporation (2021), the average time of 50% of the consolidation is around 3 years and the required time for 90% of the consolidation is around 14 years. Thus, the subgrade apparently works well under the static loading conditions.

In the area of the project, stone required for the routine subgrade is scarce and expensive. Given the difficulty to consider the role of such subgrades in designing foundations by analytical solutions, the researchers conducted several numerical analyses to check the alternative rehabilitation methods to develop an optimal design for the foundations, applying both static and seismic loadings.

[2] c_v is the coefficient of consolidation and a measure of the rate at which the consolidation process takes place

4. Numerical analyses to design foundations

Both static and dynamic analyses were conducted in numerical modeling of foundations design. The static loading included construction of the buildings and the subsequent consolidation. In the dynamic analysis, a selected input motion was applied to the whole geometry.

One-story up to four-story buildings were carefully investigated by a comprehensive numerical modeling. Grid foundations were preferred in the foundations design, grounded in the previous successful experiences of the authors (Jalili *et al*. 2022). Fig. 15 shows the model of a four-story structure over a grid foundation with a subgrade which is frequently implemented by local engineers in the project area.

In addition to the typical foundation shown in Fig. 15, to probe into functionality of the footings during and after a seismic loading, the four-story building was modeled over different foundation types and the results were compared. As shown in Figs. 15 and 16, the foundation types in the analyses are as follows:

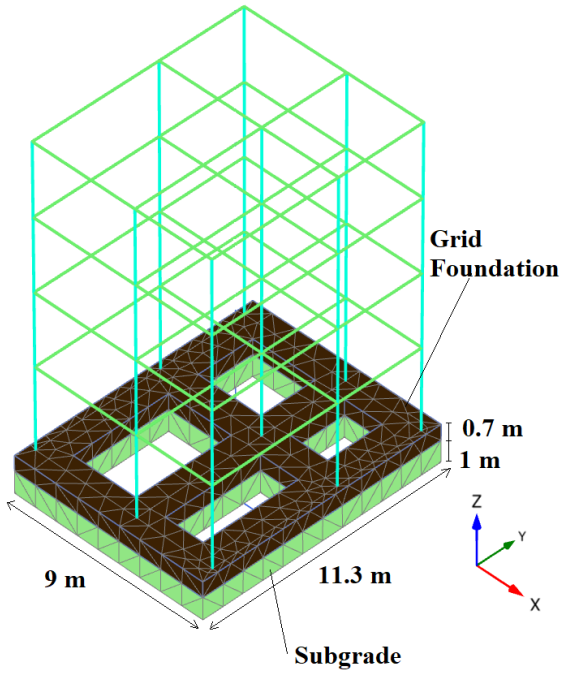

Fig. 15 Model of typical foundation on the project site: grid foundation overlying the subgrade

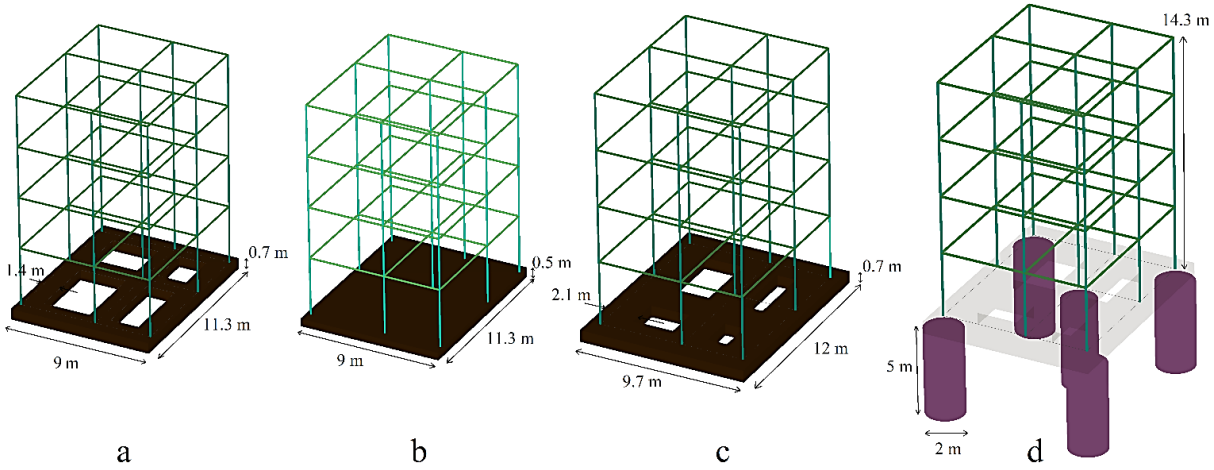

Fig. 16 Foundation types in the numerical analyses: (a) Grid, (b) Mat, (c) Widened grid and (d) Widened grid over short piles

- Grid foundation over subgrade (Fig. 15)
- Grid foundation (Fig. 16(a))
- Mat foundation (Fig. 16(b))
- Grid foundation with widened strips (Fig. 16(c))
- Grid foundation with widened strips over short piles (Fig. 16(d)).

4.1 Construction of the numerical model

Initially, the modeling of the geometry in PLAXIS finite element code (2020) as well as assignment of the material models and generation of the proper meshes took place. Then, the subsequent computational phases were defined. The construction phase was modeled in stages to build up the correct stress distribution beneath the foundations of the buildings. Finally, the input motions were applied to the bottom of the whole geometry.

With the aim to increase the accuracy of the numerical analyses, numerous factors were taken into consideration: proper modeling of the bedrock and the lateral boundaries, precise preference of the soil constitutive model, optimal preference of the dynamic time stepping and mesh size, correction of the input motions with respect to the standard regulations and the seismic hazard studies of the area (ASCE 7 2016). In the next section, a brief description of the analysis sequences and the relevant outputs are given.

4.1.1 Geometry of the buildings in 3D models

First, the soil layering under the foundation was simulated. The stratigraphy of the project site is sketched in

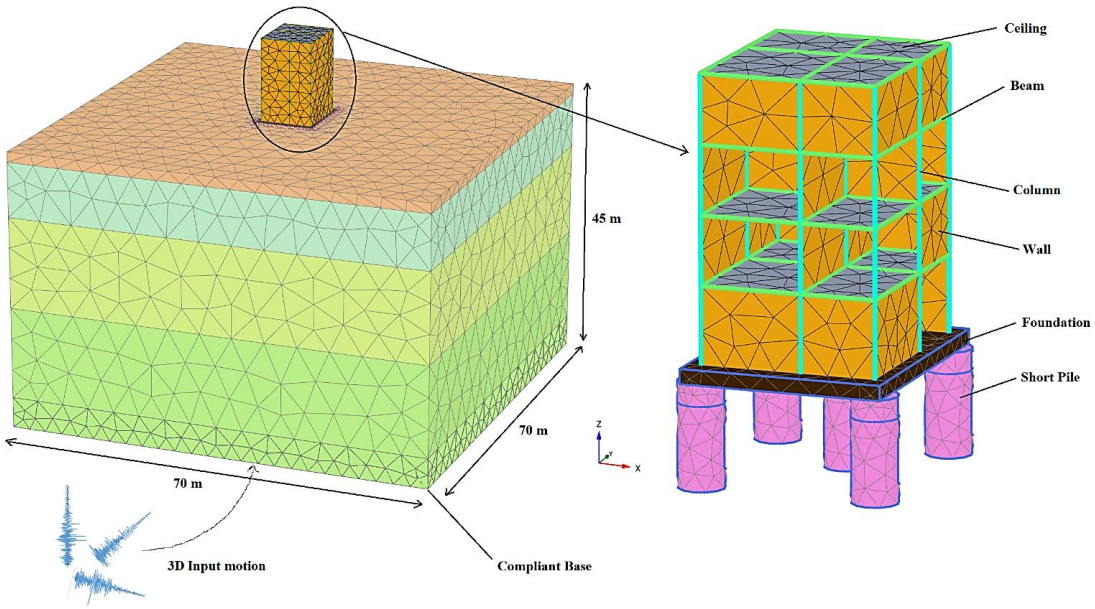

Fig. 17 Geometry of the four-story building model in the PLAXIS 3D code

Fig. 2. The foundation and the structure (including columns, beams, ceilings, and walls) were then constructed on the soil layers. The geometry of the buildings was simulated in PLAXIS 3D code as precisely as possible. Fig. 17 shows the geometry of a four-story structure. Structure details were simulated as precisely as possible to enhance soil-structure interaction in the model.

Second, the lateral boundaries of the 3D model at the foundation level were distanced 70 m from side to side in each direction to reduce unwanted reflections of the input motions during a dynamic analysis. In addition to the distant boundaries, the absorbent boundaries of the PLAXIS 3D code were also added to both of the lateral sides of the model, which reduces unwanted wave reflections (PLAXIS 2020).

Third, the bottom of the model was extended to the depth of four times the foundation width (45 m). A compliant base was defined at the bottom of the geometry which lets the input waves to refract, as well as reflect (PLAXIS 2020). Consequently, only the upward travelling part of the outcropping input motions was applied to the compliant base at the bottom of the model.

It should be noted that the seismic bedrock was nearly 100 m deep and, therefore, the model would become too large to be analyzed efficiently with such a large depth. As will be stated in the outputs of the numerical analyses, the attained acceleration time history in free field on the surface of the model was similar to the proposed input motions from seismic hazard studies (Zaferani and Rashidi 2021).

4.1.2 Soil constitutive model

Two constitutive models were used in this investigation. The Hardening Soil (HS) model was preferred for the simulation of the construction phase of the buildings because the pattern of loading in these stages is simulated by the HS model precisely (Brinkgreve *et al.* 2007).

The UBC3D-PLM model in PLAXIS3D is capable of liquefaction modeling in successive uniform cycles of loading (Petalas and Galavi 2013). This model was used for the dynamic loading analysis in this investigation.

The HS model

The HS model is based on the hyperbolic model while benefiting from the isotropic hardening in two modes of shearing and compression, both following a non-associated flow rule (Brinkgreve *et al*. 2007). The model is easily calibrated by a triaxial monotonic test, as shown in Fig. 18. The test shown in Fig. 7 is simulated in PLAXIS and the parameters that were extracted from the detailed investigation reviewed in Section 2 of this paper were used for the HS model, as mentioned in Table 2. The detailed definition of the HS parameters may be found in PLAXIS manual (PLAXIS 2020) and are not repeated herein to observe brevity.

The UBC-PLM model

The UBC-PLM model benefits from the Mohr-Coulomb yield function with isotropic hardening and a secondary yield surface with a simplified kinematic hardening rule and a non-associated flow rule grounded in the Drucker-Prager plastic potential function (Petalas and Galavi 2013), enabling the model to differentiate between the primary and secondary loading. The model employs a densification law through the secondary yield surface with a kinematic hardening rule that improves the precision of the generation of excess pore water pressure.

Contrary to the calibration of the HS model which was built on the monotonic triaxial test results, when it comes to the UBC-PLM model, the suggested correlations with SPT values (Makra 2013) and the default values suggested by Petalas and Galavi (2013) were considered. The authors have experienced that by way of calibrating the UBC-PLM

Table 2 HS material model parameters used for modeling foundation soil

Parameters	Description	(Unit)	Value
Drainage	drainage type	-	Undrained
$\gamma_{unsaturated}$	unsaturated unit weight	kN/m^3	18
$\gamma_{saturated}$	saturated unit weight	kN/m^3	19
E_{50}^{ref}	average secant stiffness in standard drained triaxial test	kN/m^2	5000
E_{oed}^{ref}	tangent stiffness for primary oedometer loading	kN/m^2	2500
E_{ur}^{ref}	unloading / reloading stiffness	kN/m^2	19000
m	Power for stress-level dependency of stiffness	-	1
C	(effective) cohesion	kN/m^2	21
φ'	(effective) angle of internal friction	°	20
ψ	angle of dilatancy	°	15
c_c	compression index	-	0.17
e_0	initial void ratio	-	0.7
k	permeability	m/s	10^{-10}

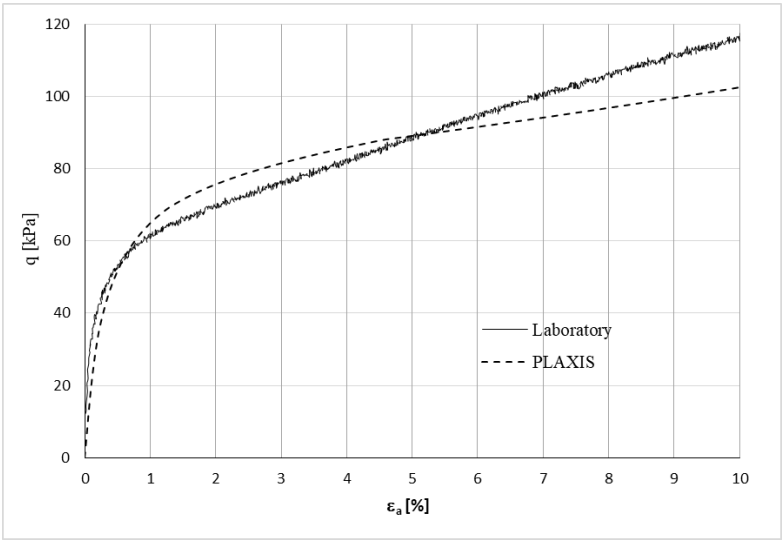

(a)

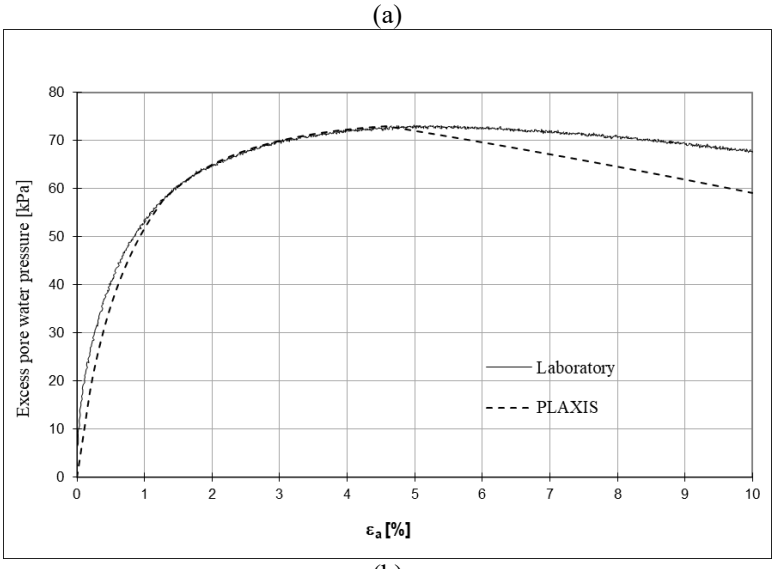

(b)

Fig. 18 Calibration of the HS constitutive model in PLAXIS with the triaxial test data from laboratory: (a) deviator stress versus axial strain and (b) excess pore water pressure ratio versus axial strain

Table 3 UBC3D-PLM material model parameters used for dynamic analysis of models

Parameter	Description	Units	Values		
			shallow	deep	deeper
Drainage	drainage type	-	undrained	undrained	undrained
ϕ_{cv}	constant volume friction angle	Degree	20	20	20
ϕ_p	peak friction angle	Degree	21	26	32
c	cohesion	kN/m^2	20	20	30
k_G^e	elastic shear modulus factor	-	879	1347	1597
k_G^p	plastic shear modulus factor	-	431	3737	12080
k_B^e	elastic bulk modulus factor	-	615	943	1118
m_e	rate of stress-dependency of elastic bulk modulus	-	0.5	0.5	0.5
n_e	rate of stress-dependency of elastic bulk modulus	-	0.5	0.5	0.5
n_p	rate of stress-dependency of plastic shear modulus	-	0.4	0.4	0.4
R_f	failure ratio	-	0.8	0.7	0.6
P_A	reference pressure	kN/m^2	100	200	400
σ_t	tension cut-off and tensile strength	kN/m^2	0	0	0
γ_{unsat}	unsaturated unit weight	kN/m^3	19	18	20
γ_{sat}	saturated unit weight	kN/m^3	20	19	21
fac_{Hard}	densification factor	-	1.0	1.0	1.0
$(N_1)_{60}$	corrected SPT value	-	9	30	50
k	permeability	m/s	10^{-10}	10^{-10}	10^{-10}

Table 4 Properties of beam and column elements

Type	Unit weight	Cross section area	Young's modulus in axial direction	Moment of inertia against bending around the second axis	Moment of inertia against bending around the third axis
	γ [kN/m^3]	A [cm^2]	E [kPa]	I_2 [m^4]	I_3 [m^4]
Beam	0.25	780	$24.94*10^6$	$0.512*10^{-3}$	$0.512*10^{-3}$
Column	0.25	924	$24.94*10^6$	$0.603*10^{-3}$	$0.830*10^{-3}$

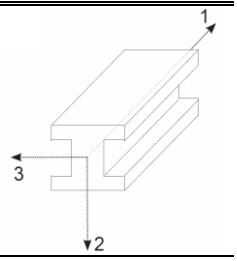

by these correlations seismic events can be simulated more exactly, compared with calibrations based on cyclic test results (Moradi and Jalili 2022). Given the variation of SPT values in relation to depth, three different sets of parameters were considered for 1-10 m, 11-25 m, and 26-45 m. They are called shallow, deep, and deeper, respectively, as shown in Table 3. A detailed definition of the parameters can be found in Petalas and Galavi (2013), not given herein for the sake of brevity.

Beams and columns of the structure were modeled elastic, which lead to concentration of non-linearity in the underlying soil and consequent conservative settlements. Table 4 contains properties of beams and columns.

4.1.3 Mesh dimensions

In defining the proper mesh size for the dynamic analysis, it is crucial to observe that the largest mesh dimension should not be more than $\frac{1}{12}$ of the shortest wave length, as noted by Lysmer and Kuhlemeyer (1969). In addition to this criterion, to prefer the optimal mesh size a harmonic pulse was applied to the geometry and the vibration amplitude of the building foundation was compared, rerunning the analysis with different mesh sizes. The optimal mesh size is depicted in Fig. 17.

4.1.4 Input motion

Input motion was selected in accordance with the results of the obtained seismic hazard analyses of the area. The motion was recorded at the same tectonic region and with identical faulting mechanism as in the present study. Fig. 19 shows the input motion used in this study. Three recorded components of the motion called 3241 (L, T and V components) with properties mentioned in Table 5, were applied in X, Y and Z directions, respectively, as shown in Fig. 17.

Table 5 shows the main characteristics of the input motion called 3241.

4.2 Static numerical analyses results

According to the Iranian national building code (7th issue, 2013), the maximum allowable mat or grid

Table 5 Main characteristics of the input motion called 3241

Earthquake	Station	Magnitude	Mechanism	Distance (km)	Vs30 [m/s]	PGA [gal]
3241	Ahram (Zagros)	5.1	Reverse	12	988	170

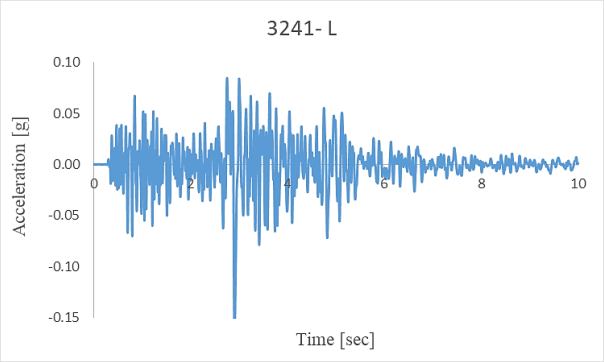

(a)

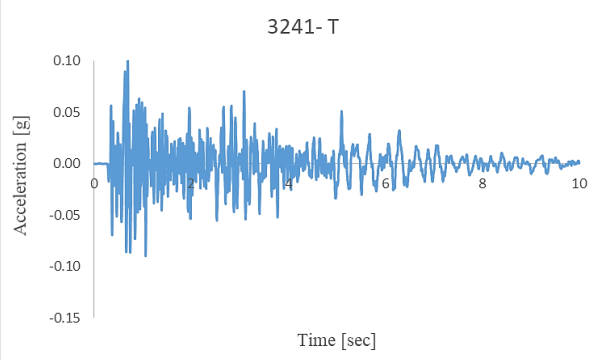

(b)

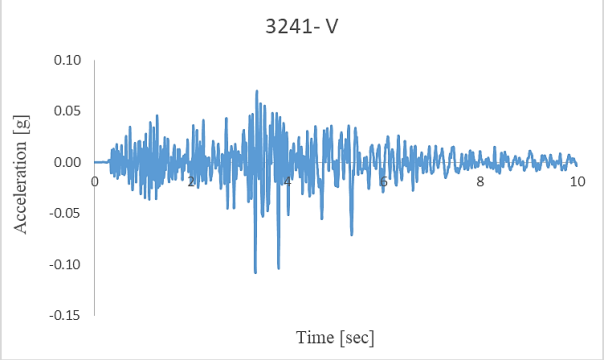

(c)

Fig. 19 Three components of the recorded input motion "3241" used in this study: (a) Record 3241-L in X direction, (b) Record 3241-T in Y direction and (c) Record 3241-V in Z direction

foundation settlement over coarse-grained and fine-grained soils is 5 cm and 6.5-10 cm, respectively.

Fig. 20 shows the results of the consolidation analysis of the one-story to four-story structures on grid foundation on subgrade (Fig. 15). In a performance-based design approach, it was decided to allow the excessive settlement to dissipate during the construction period, leading to allowable settlement during the life-time span of the structure. To be conservative, we considered 4 cm allowable settlement during the life-time span of the structure.

Consequently, the minimum construction period was considered in the way depicted in Fig. 19. The time required to dissipate the excessive settlement (over 4 cm) during the construction was 3 months for one-story structure, and 12 months for the four-story structure. In the authors' opinion, this is why the current buildings in the area of the project do not suffer from excessive settlement. The point of importance is that the relatively slow rate of construction can dissipate a large portion of the settlement.

4.3 Dynamic numerical analyses results

As stated in Section 4.1.1, only the upward travelling part of the outcropping input motions were applied to the compliant base at the bottom of the model. Fig. 19 shows this upward traveling part which is imposed to the model. Fig. 21 shows the recorded output of the model, which is the acceleration time history and its response spectra at three different locations of the numerical model: at the compliant base, on the ground surface (distant from the building in a free-field condition) and also on the grid foundation beneath the building. The recorded data at the compliant base is the combination of both the upward and downward traveling parts of the refracted and reflected waves at the base.

The seismic hazard analyses of the project area establish the peak rock acceleration as 0.16 g and the peak ground acceleration as 0.22 g (Zaferani and Rashidi 2021). Fig. 21 depicts that the motions at the bottom of the model and on the surface of the ground have the same maximums as those expected.

The spectral accelerations in Fig. 21 show that even though amplification of input motions occur when the wave arrives at the surface, the interaction of the building with the underlying soil reduces the amplitude of the motion, compared with the free-field motion. Due to the interaction of the three orthogonal components, it is not easy to judge the frequency content of the soil body and the foundation by way of comparing the response spectra of the surface and the base.

The settlement of the four-story structure over different foundations (in Fig. 16) is shown in Fig. 21. All the observed settlements in the numerical simulations of this study were uniform across the entire foundation. Consequently, the magnitudes shown in Fig. 22 show rigid and uniform settlement of the whole foundation.

Crucially, due to the settlement of the entire soil body of the model, different counting measures against extra settlement are practically similar in seismic loading. Even though the input motion amplitude is not considerably large (0.15 g in X direction and 0.1 g in Y and Z directions), continuous shaking of the soil shifts it to the softening phase, leading to 6 cm settlement.

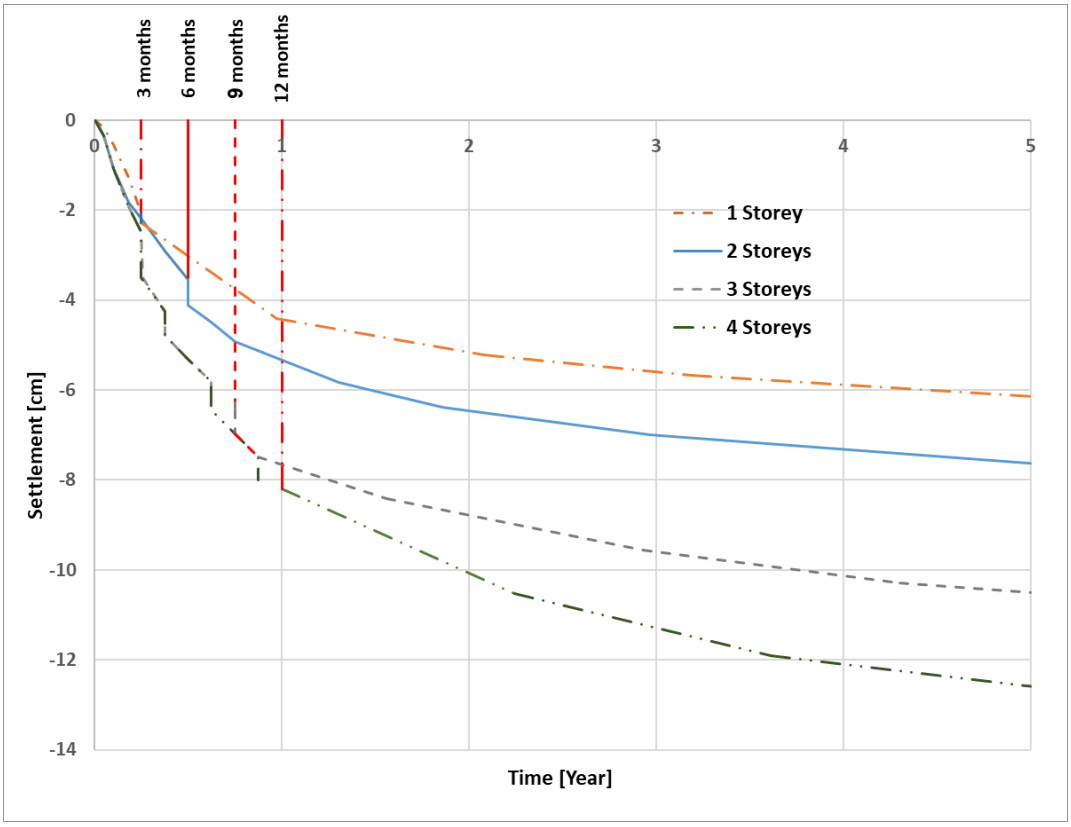

Fig. 20 Settlement of one-story to four-story buildings' numerical model during consolidation phase

5. Factor of safety against cyclic softening

The approach of safety factor evaluation against liquefaction (Kramer 1996) was followed in this study to find out the safety against cyclic softening. The cyclic stress ratio (shear stress/effective vertical stress) which was required to cause cyclic softening (called cyclic resistance ratio or CRR herein) was compared to the cyclic shear stress ratio induced by earthquake (called CSR herein) to evaluate the safety factor. A point of importance is that CRR should be greater than CSR to avoid softening. CRR=0.25 was evaluated from the cyclic triaxial tests, as stated in Section 2.2. This CRR is for the free-field condition. For the soil below the foundation of the structure, a preliminary permanent static shear stress is applied to the soil. Boulanger and Idriss (2007) have proposed a correction factor for this static stress called K_α, which was used herein.

To extract K_α, the static shear stress was estimated by the aid of numerical analyses described in Section 4.2, as shown in Fig. 23. To avoid ambiguities regarding 3D geometry, only one plane (Z-X) was considered to extract K_α. Fig. 23(a) shows the distribution of shear stress in Z-X plane, in a section of the grid foundation under the four-story building. The distribution of the effective vertical stress under the grid foundation under the four-story building is also shown in Fig. 2(b). CRR was 0.18 to 0.22 in the first 10 m (a depth equal to the width of the foundation) below the foundation, according to the stress distribution in Fig. 23.

To evaluate CSR, the results of the detailed 1D site response analyses conducted by the authors were considered. DEEPSOIL code (Hashash *et al.* 2020) was used and shear stress distribution was calculated along the initial depths of several representative geotechnical profiles of the project area. The details of site response analyses are out of the scope of this paper. Only the relevant outputs are reported herein. Fig. 24 shows the distribution of shear stress along the profiles that are spread all over the project area. The average CRR at the first 5 m is smaller than the CSR and, consequently, this zone is prone to cyclic softening, as depicted in Fig. 24.

Based on the simplifying assumption of constant 3.5% single amplitude of strain throughout the softened layers (Section 2.2), the volumetric strain after softening can be nearly 1.5% (Kramer 1996). Consequently, the amount of the settlement due to the softening shown in Fig. 24 would be estimated as 7.5 cm. It is worthwhile to notice that the dynamic numerical analyses on the same foundation and structure produce an amount of foundation settlement (6 cm in Fig. 22) which is nearly similar to the above estimate.

For such a considerable amount of settlement, ground modification methods can be a solution, as pointed out in the introduction. Given all the factors including soil type and the local constructors' skills, three methods were preferable over other choices in this study:

- Deep Soil Mixing
- Jet Grouting
- Stone Column (Vibro-replacement)

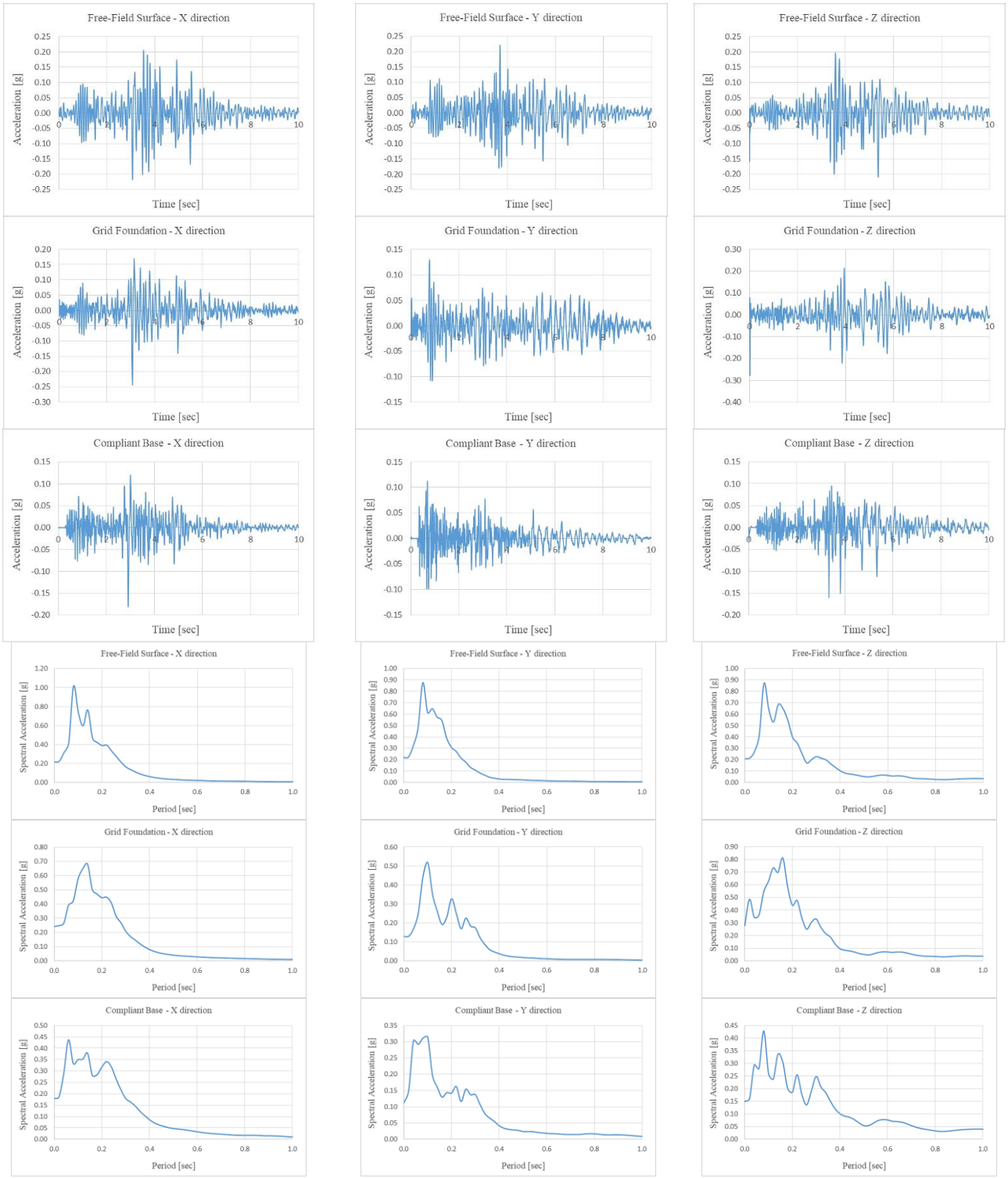

Fig. 21 Acceleration time history and acceleration response spectra of the ground surface (free-field), compliant base of the model and the grid foundation

As mentioned previously, it was not economically possible to perform any of these methods of modification due to the vast area of the project.

The final decision was to keep following the performance-based design approach, as implemented in the static design. In addition to the time schedule of the construction established in the static design (Fig. 20), the structure of the four-story and three-story buildings had to be strengthened with a slab of reinforced concrete as a stiffener. The slab was constructed directly over the foundation to guaranty a uniform settlement of the building.

Crucially, the inclusion in this stage of the subgrade and

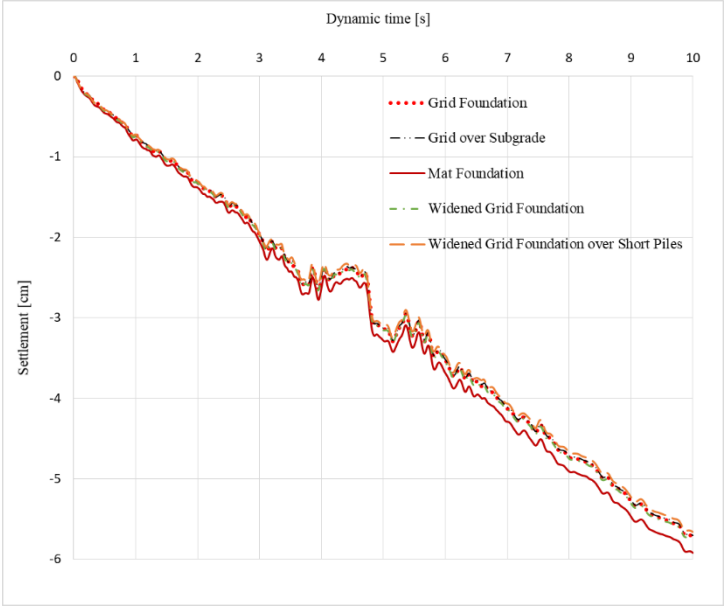

Fig. 22 Settlement of four-story building over different types of foundations in the seismic analyses

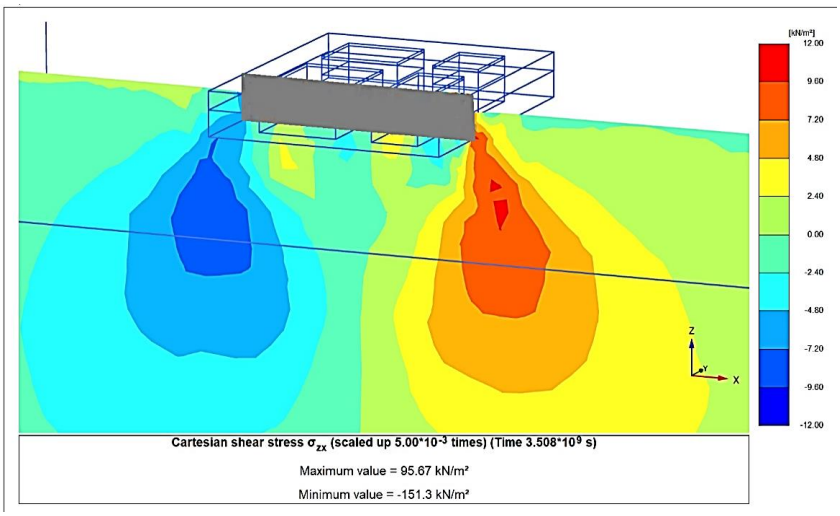

(a)

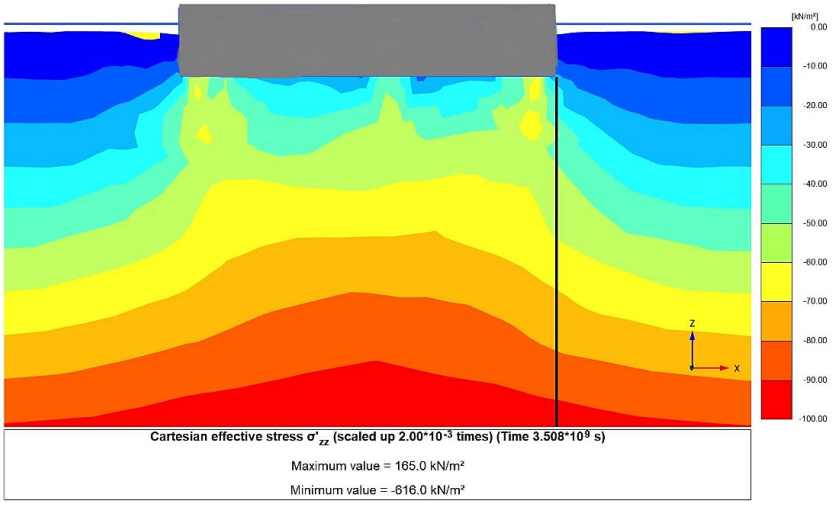

(b)

Fig. 23 Stress distribution under the foundation of the four-story building: (a) Shear stress distribution in a section in Z-X plane and (b) Effective vertical stress in the same section

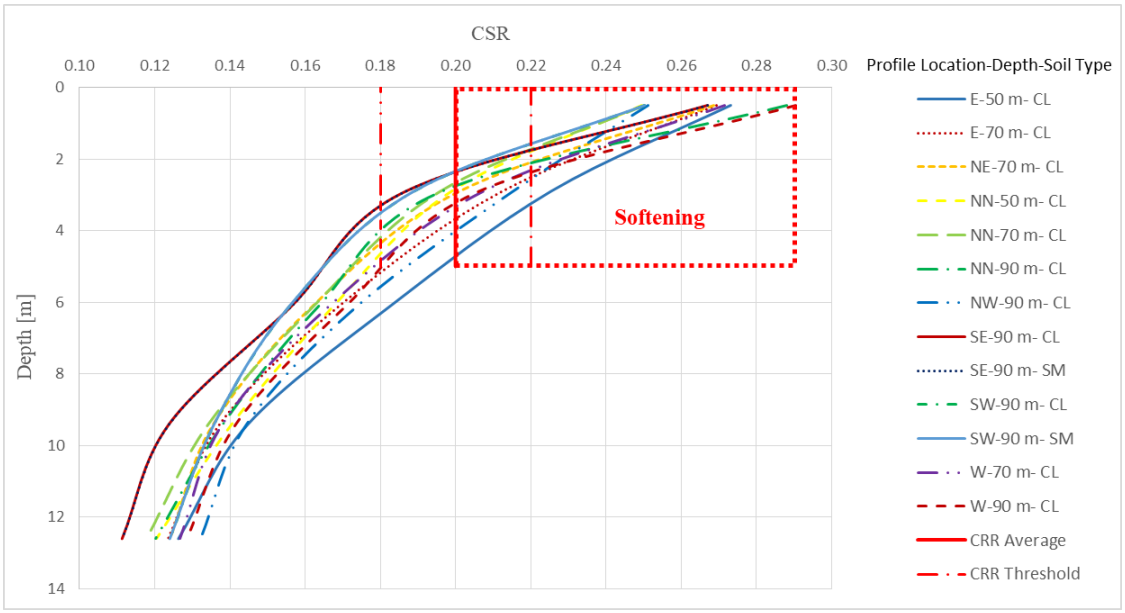

Fig. 24 Shear stress ratio along the initial depths of the representative geotechnical profiles across the project area

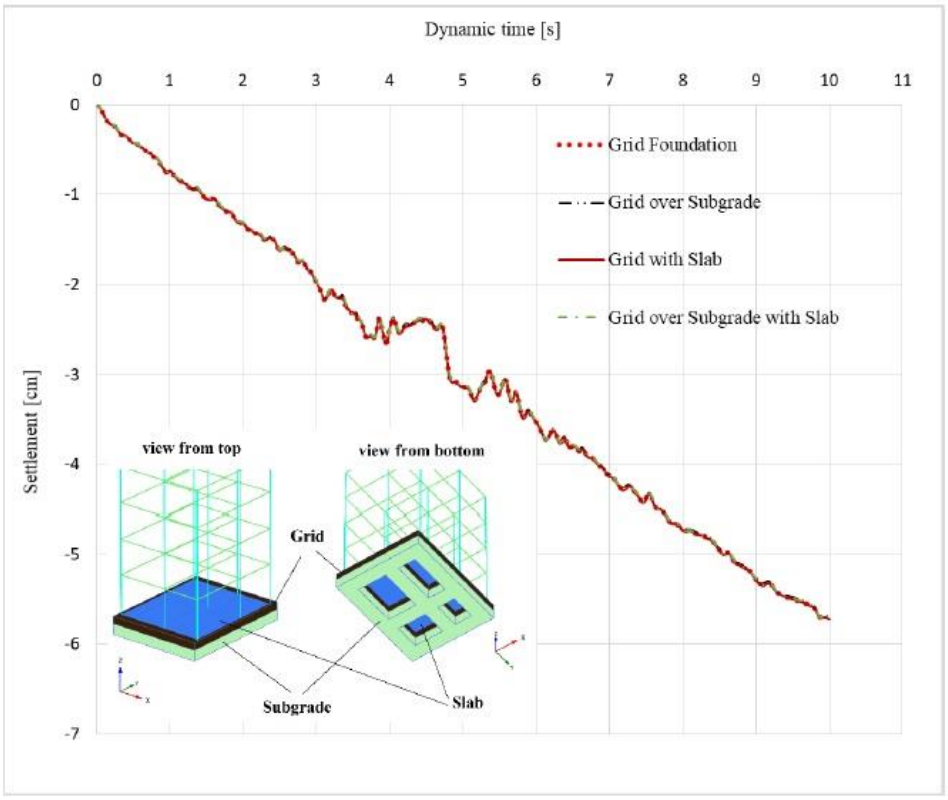

Fig. 25 Settlement of four-story building over different types of foundations in the seismic analyses

the slab to the numerical model did not change any of the results obtained when they were excluded. Fig. 25 shows the settlement of the grid foundation with and without the subgrade and the slab. However, despite the homogenous and isotropic soil model in the numerical analyses, the consistency of the soil beneath a foundation may vary. Taken together, the use of the subgrade and the slab are practically evidenced as an increase in the factor of safety against potential structure collapses in differential settlements.

Lastly, the owners of the constructed houses were informed that in case an earthquake of the strength of the present design takes place, the structures may experience a substantial amount of settlement, yet indicating resistance against a collapse. The foundations of the relevant constructed houses rest on the ground surface, leveling the

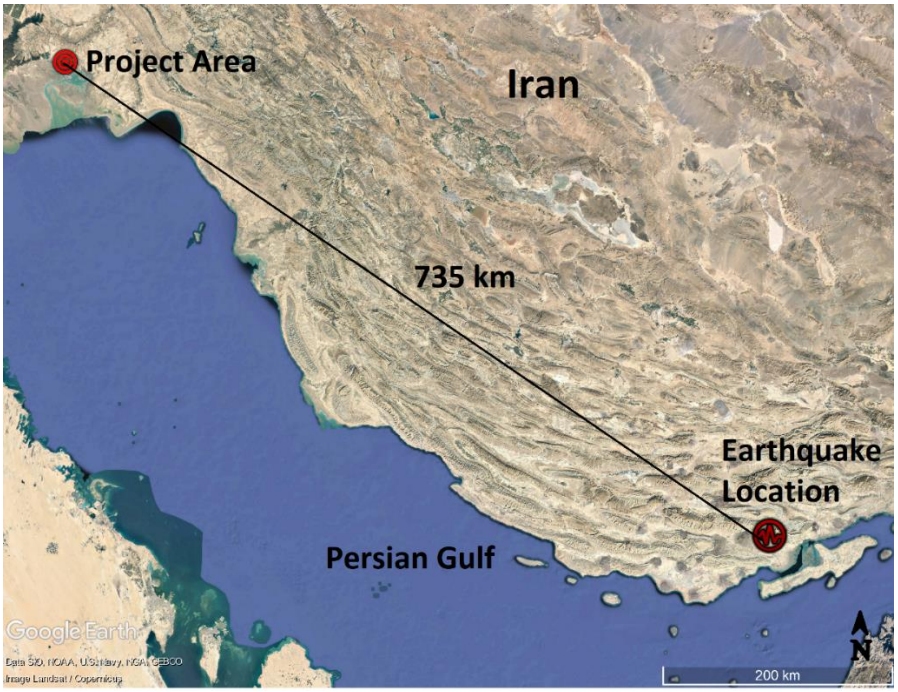

Fig. 26 Location of two earthquakes in Sayeh Khosh

structure 0.7 m above the ground (similar to Fig. 14).

6. Field evidence of the behavior of different types of foundations

During the preparation of this manuscript, two large earthquakes occurred on July 1, 2022, in another coastal region of the Persian Gulf, approximately 735 km east of the study area reported on here. These earthquakes, the first one with magnitude (M_L=6.1) and the second one with magnitude (M_L=6.2), struck severely Sayeh Khosh village and the surrounding region between Khamir and Lengeh ports in Hormozgan province at the interval of nearly 1 hour (IIEES, 2022). Fig. 26 shows the location of the earthquakes and its vicinity to the site of the present project.

Based on observations of the IIEES reconnaissance team (Haghshenas *et al*. 2022), the two earthquakes induced an extensive liquefaction and lateral spreading in a wide-spread area south of the Sayeh Khosh village (Fig. 27). From the geological point of view, this region typically has fine-grained sandy soils, deposited on the delta of the Mehran River. There is a clear difference between the geological settings of this region and the area studied in the present paper. The former has fine-grained sandy soils, the latter silty-clayey soils. Despite this difference the building structures were affected in a similar way in terms of excessive settlement. As a consequence, the noteworthy point is that the performance-based design approach proved efficient during the above-mentioned earthquakes with high magnitudes. Figs. 28 and 29 presented by Haghshenas *et al*. (2022) show an area 8 kilometers away from the epicenter of the earthquakes. Those buildings, that were designed stiff, experienced a nearly 20 cm settlement without a considerable damage to the building. Fig. 28 depicts that in some cases the residents continued to use the quake-stricken building, after fixing the major damage.

In contrast to those buildings that did not suffer too heavy damage, the buildings that were not stiff enough to tolerate excessive settlements, were destroyed unfortunately. Fig. 29 shows one of the damaged buildings due to the excessive settlement of the underlying liquefied soil.

Detailed information about the soil classification and the foundation of the buildings in Figs. 28 and 29 is not available, yet. This report is only a qualitative preliminary presentation of the effects of the violent earthquakes. Relating to the present project, the event of the violent earthquakes explicitly supports the need to design rigid foundations for buildings to tolerate excessive settlements without demolishing damage.

7. Conclusions

This study aimed to economically design foundation of several buildings resting on soft compressible soils that are susceptible to cyclic softening, relying on comprehensive experimental, theoretical and numerical investigations. The main findings are:

- Soft compressible soil with extensive settlement due to building construction may still be safe by a proper construction schedule. It can dissipate most of the settlement during construction.
- Proper numerical analyses facilitate the development and implementation of improvement of the classical analytical design of foundations by making it possible to simulate retrofits, such as a rigid subgrade.

Fig. 27 Liquefaction and lateral spreading due to the Sayeh Khosh earthquakes in the nearby areas

Fig. 28 A stiff building that tolerated nearly 20 cm settlement without considerable damage

Fig. 29 A damaged building that could not tolerate excessive settlement

- Even though clayey soils are not susceptible to liquefaction, they may suffer from cyclic softening and experience considerable settlement.
- Dynamic numerical analyses give results for settlements similar to those estimated by the empirical relationships in the literature on liquefaction, if proper constitutive modeling with appropriate calibration is used.
- In the absence of massive ground modifications due to economical limitations, local retrofits, such as a subgrade or short piles under the foundation which can be described as floating in the soft compressible soil that is prone to softening, do not reduce settlements. Due to the shaking of the area, the whole site soil settles, including the floating foundations and its subgrade.
- A solution would be to have a proper estimate of the pre- and post-earthquake settlements to consider a proper schedule of construction, in addition to providing appropriate rigidity for the foundation.
- Subgrades made of stone and lime mortar placed under the foundation and a slab of reinforced concrete on the foundation were observed in this study to provide sufficient rigidity for the foundation of the structures to survive substantial amounts of settlements.
- The proposed design method in this study is much cheaper than routine soil-improvement methods, that makes it worth noting as an alternative in design of foundations on deep strata of soft and compressible fine-grained soils in areas prone to earthquakes.

Acknowledgements

This study was supported partly by the International Institute of Earthquake Engineering and Seismology (IIEES) and partly by the Natural Disasters Research Institute (NDRI). The authors gratefully acknowledge the IIEES and NDRI as well as Mrs. Rakhshande for the valuable data she gathered from the field observations. Dr. M.K. Jafari and Dr. M. Davoudi are highly acknowledged for their valuable help during the research. The authors also thank Mr. M. Asgari, Mr. G. Hadavi and Mr. S. Azadmanesh for their assistance in conducting the tests.

References

American Society of Civil Engineers, and Structural Engineering Institute, (2016), *Minimum Design Loads on Buildings and Other Structures*, Standards Committee.

Boulanger, R.W. and Idriss, I.M. (2004), "Evaluating the potential for liquefaction or cyclic failure of silts and clays", (p. 131). Davis, California: Center for Geotechnical Modeling.

Boulanger, R.W. and Idriss, I.M. (2007), "Evaluation of cyclic softening in silts and clays", *J. Geotech. Geoenviron. Eng.*,

133(6), 641-652. https://doi.org/10.1061/(ASCE)1090-0241(2007)133:6(641).

Bowles, J.E. (1996), *Foundation Analysis and Design*, 5th Ed., McGraw-Hill Companies.

Brinkgreve, R.B.J., Kappert, M.H. and Bonnier, P.G. (2007), "Hysteretic damping in a small-strain stiffness model." *Proceedings of the Numerical Modeling in Geomechanics*, NUMOG X, Rhodes:737-742.

Brinkgreve, R.B.J., Swolfs, W.M. and Engin, E. (2020), *PLAXIS User's Manuals*, PLAXIS BV, Delft, The Netherlands.

Building and Housing Research Center. (2014), *Iranian Code of Practice for Seismic Resistant Design of Buildings, Standard No. 2800*. Fourth Revision, Tehran, Iran.

Coduto, D.P., Kitch, W.A. and Yeung, M.C.R. (2014), *Foundation design: principles and practices*. USA: Prentice Hall.

Day, R.W. (2010), *Foundation engineering handbook: design and construction with the 2009 international building code*. McGraw-Hill Education.

Fakher, A. (2011), *Advanced Foundation Engineering*, 1st edition University of Tehran press (in Persian).

Ghazavi, M. and Hadiani, N. (2005), *Bearing capacity of multi-edge shallow foundations*. M.Sc. thesis, K. N. T. University of technology, Tehran, Iran (in Persian).

Ghazavi, M. and Mokhtari, S. (2008), "Numerical investigation of load-settlement characteristics of multi-edge shallow foundations", *Proceedings of the 12th International Conference of International Association for Computer Methods and Advances in Geomechanics*, Goa, India.

Hashash, Y.M.A., Musgrove, M.I., Harmon, J.A., Ilhan, O., Xing, G., Numanoglu, O., Groholski, D.R., Phillips, C.A. and Park, D. (2020), *DEEPSOIL 7.0, User Manual*. Urbana, IL, Board of Trustees of University of Illinois at Urbana-Champaign.

Hodgkinson, A. (2013), *Foundation Design*. Elsevier.

Jalili, J., Askari, F., Haghshenas, E., Zaferani, H., Rashidi, A. and Davoudi, M. (2021), *Comprehensive geotechnical studies on the site of Sarbandar city in Khuzestan province, to suggest improvement methods with seismic considerations*. Research report at International Institute of Earthquake Engineering and Seismology, Iran (*in Persian*).

Karstunen, M. and Leoni, M. (Eds.) (2008), "Geotechnics of Soft Soils: Focus on Ground Improvement", *Proceedings of the 2nd International Workshop* held in Glasgow, Scotland, 3-5 September 2008. CRC Press.

Kramer, S.L. (1996), *Geotechnical earthquake engineering*. Pearson Education India.

Lysmer, J. and Kuhlemeyer, R.L. (1969), "Finite dynamic model for infinite media", *J. Eng. Mech. Div.*, **95**(4), 859-878. https://doi.org/10.1061/JMCEA3.0001144.

Makra, A. (2013), *Evaluation of the UBC3D-PLM constitutive model for prediction of earthquake induced liquefaction on embankment dams*. Master graduation thesis, Delft University of technology.

Moradi, M. and Jalili, J. (2022), "Investigation on the 2D and 3D numerical simulation of centrifuge tests on a soil-nailed wall under seismic loading", *Bulletin of Engineering Geology and the Environment*, under review.

Petalas, A. and Galavi, V. (2013), *PLAXIS liquefaction model ubc3d-plm*, PLAXIS Report.

Road, Housing and Urban Development Research Center. (2013), *Iranian National Building Code, 7th issue, Foundation Design and Construction*, Tehran, Iran.

SakhtAzma geotechnical consulting engineers. (2021), *Report of subsurface investigation-Imam Khomeini Port (Sarbandar)*, Khuzestan, Iran.

Schaefer, V.R., Berg, R.R., Christopher, B.R., DiMaggio, J.A., Filz, G.M., Bruce, D.A., Ayala, D., Collin, J.G. and Berg, R.R. (2016), *Geotechnical Engineering Circular No. 13 Ground Modification Methods-Reference Manual*, Volume II (No. FHWA-NHI-16-028). National Highway Institute (US).

Seed, R.B., Cetin, K.O., Moss, R.E., Kammerer, A.M., Wu, J., Pestana, J.M., Riemer, M.F., Sancio, R.B., Bray, J.D., Kayen, R.E. and Faris, A. (2003), "Recent advances in soil liquefaction engineering: a unified and consistent framework." *In Proceedings of the 26th Annual ASCE Los Angeles Geotechnical Spring Seminar*: Long Beach, CA.

Zamiran consulting engineers. (2002), *Soils and foundations investigation, proposed PVC complex, for Ghadir petrochemical company*, Iran.

IC